Addendum to the PI-SWERL Report of Etyemezian et al. (2014)

Particle Size Distribution Characteristics and PI-SWERL® PM_{10} Emission Measurements: Oceano Dunes State Vehicular Recreation Area

J.A. Gillies and V. Etyemezian
Division of Atmospheric Sciences, Desert Research Institute, Reno and Las Vegas, NV

Report Prepared for:

Oceano Dunes State Vehicular Recreation Area
Off-Highway Motor Vehicular Recreation, California State Parks, 1725 23rd Street, Suite 200, Sacramento, CA 95816

Introduction

As part of the 2013 wind erodibility measurements at the ODSVRA, the PI-SWERL™ instrument (Etyemezian et al., 2007, 2014a) was used to measure dust emission potential (Etyemezian et al., 2014b). Intensive field measurements using two PI-SWERL™ units began on August 26, 2013 and ended on September 5, 2013. In total, 360 individual PI-SWERL™ tests were completed among the two units used, with each responsible for one-half of the total. At each test location a sample of the sand (≈300 g) was collected from around the footprint of the PI-SWERL™. A sub-set of these samples was selected for particle size analyses to define the percent sand, silt, and clay, five size classes of sand, and 162 size classes for the material that passed through (by washing) a 63 μm sieve.

The purpose for collecting the sediment samples and developing a detailed characterization of the particle size distribution (PSD) was to examine if there were characteristics of the PSD that could be linked with the strength of the dust emission potential as measured with the PI-SWERL™. Three plausible hypotheses (and probably more) can be stated to explain the source of the PM_{10} released from the sand as it saltates driven by the on-shore winds at the ODSVRA. Hypothesis one is: the source of the PM_{10} in the sand lies in a reservoir of particles that are contained within the sand (or are adhering to the sand). Here, no assumption is furnished on how the PM_{10} was formed only that it is within the sand matrix of the dunes at the time of windblown events. Hypothesis two is: the PM_{10} is created during the saltation process by the breakdown of (larger) particles due to the vigorous collisions between the particles and the surface that takes place during saltation. Hypothesis three is that hypothesis one and two are both correct: the source of the PM_{10} in the sand lies in a reservoir of particles that are contained within the sand (or are adhering to the sand) and the PM_{10} is also created during the saltation process by the breakdown of (larger) particles due to the vigorous collisions between the particles and the surface that takes place during saltation. The strength of dust emissions has been linked to soil textural properties (e.g., Gillette, 1976, 1978; Nickling and Gillies, 1989; Rajot et al., 2004) and the production of dust by the breakdown of particles and aggregates has been reported by Bullard et al. (2004, 2007), Bullard and White (2005), and Kok (2011).

Methods

Sand samples (≈300 g) associated with the PI-SWERL™ testing were collected by scooping the sand around the PI-SWERL™ to a depth of approximately 1 cm and placing it into a sealable plastic bag labeled with the PI-SWERL™ test ID. The samples were returned to Reno for analysis. Ninety one (91) samples were selected to broadly represent the geographic distribution of PI-SWERL™ measurements (Fig. 1). The samples were analyzed at the DRI Soil Characterization Laboratory.

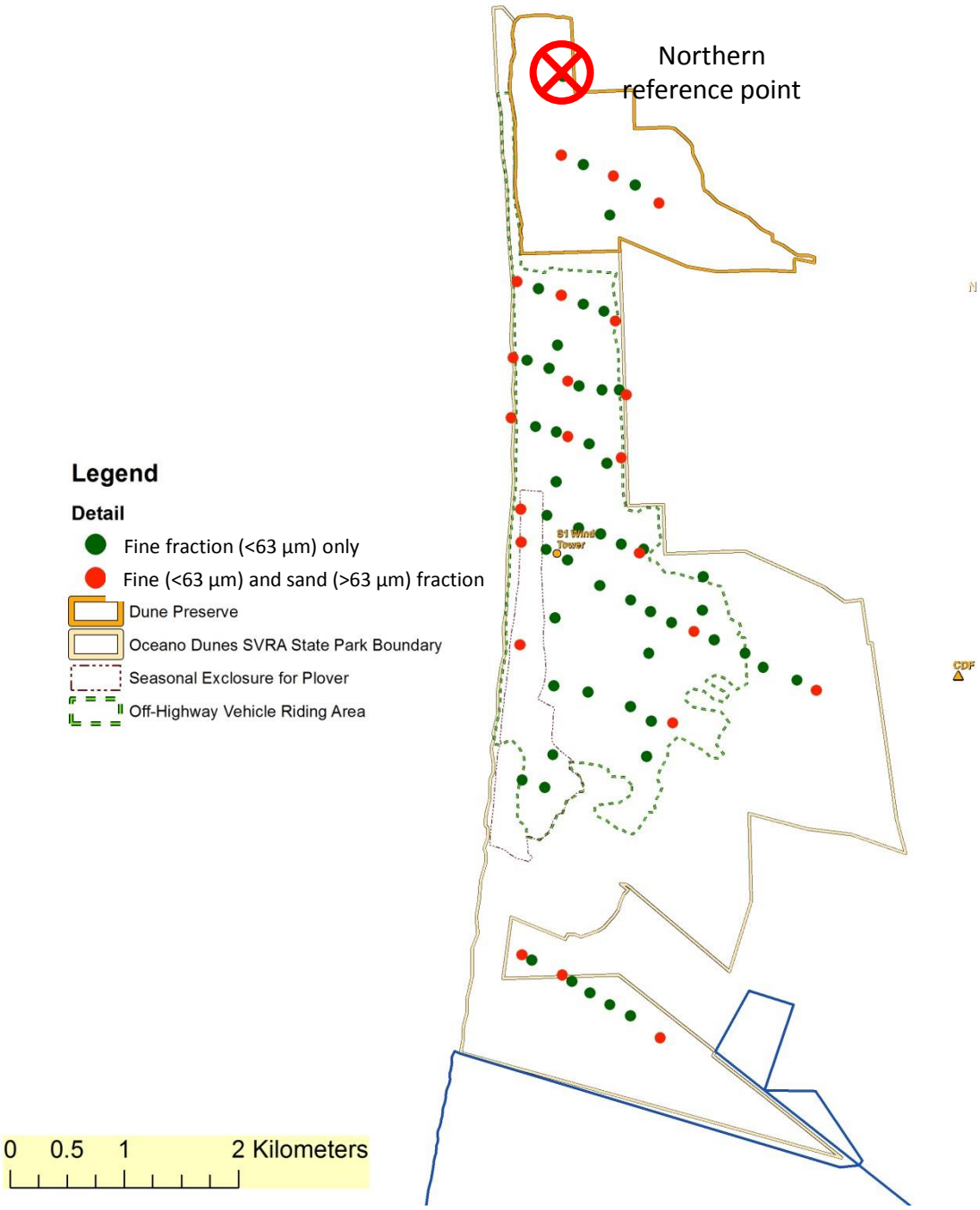

Figure 1. The locations of samples analyzed using the Malvern Multisizer (green dots) to quantify the fine fraction (<63 µm diameter) in the sand and those analyzed by sieve and Malvern Multisizer (red dots) to quantify the fine fraction (<63 µm diameter) and the coarse (>63 µm diameter) fraction. .

Each sample was weighed, oven dried overnight, allowed to cool, and reweighed to determine the water content. The dried samples were sieved through a 2 mm sieve, to determine the gravel content. Then a split of the <2 mm fraction was made (about 5-6 g). This fraction was put in a conical flask, a dilute surfactant was added, and the flasks were gently agitated overnight to break up any aggregates. The dispersed split was then wet sieved through a 63 µm sieve. The material caught in the sieve (the sand) was put into a pre-weighed dish, dried, and then weighed.

The material that passed through the sieve (the silt and clay) was put into a Malvern Mastersizer for laser particle size analysis, which has 162 size bins (0.097 µm to 1029.2 µm). The percent difference between sequential particle bin diameters is approximately 6%. The technique of laser diffraction is based on the principle that particles passing through a laser beam will scatter light at an angle that is related to their size: large particles scatter at low angles, whereas small particles scatter at high angles. The laser diffraction is described by the Fraunhofer Approximation and Mie theory, with the assumption of spherical particle morphology (Eshel et al., 2004). The percent volume fractions reported by the Malvern instrument were renormalized to account for the percent of the total (<2 mm) sample that was removed by sieving. In addition to the 91 samples, nine replicate samples were run. The mean percentage difference between replicates was 5% (±4%).

Twenty-two (22) of the samples were selected for additional analysis of the sand size fraction retained on the 63 µm sieve. The sand was dried, weighed, and sieved into five size classes: 0.0625-0.125 mm, 0.125-0.25 mm, 0.25-0.5 mm, 0.5-1.0 mm, 1.0-2.0 mm. The mass fraction values in each size bin were used to calculate the sample statistics (i.e., mean, sorting [standard deviation of the mean], skewness and kurtosis) using the publicly available particle size analysis program Gradistat (Blott and Pye, 2001).

Results

Particles >63 µm in Diameter

The separation of the particles by wet sieving showed that for all 91 samples the percentage of the material that was greater in size than 63 µm was between 97.4% and 99.6%. The mean was 99.1% with a standard deviation of 0.4%.

As expected for dunes, the texture of all samples is designated as sand. It ranges from very well sorted fine sand to moderately well-sorted coarse sand. The percent occurrence based on sediment naming conventions is shown in Fig. 2 along with the mean particle diameter for the samples in each of these categories. The samples are dominated by well sorted fine sand (36%) and moderately well sorted medium sand (27%). The corresponding mean particle diameters for these samples are 260 µm (±13 µm) and 430 µm (±27 µm), respectively. The sorting describes how even the particle size distribution is (Fig. 3), which in the case of the two most frequently occurring sand type samples is well sorted and moderately well sorted. The aeolian sediment transport process, i.e., saltation, tends to sort the grain size distribution as a function of particle size along the direction of transport. As wind initiates the transport process, the smaller sized particles are mobilized at lower speeds and then move downwind more quickly than the less easily entrained heavier particles that move downwind more slowly (those in creep mode for example). This process leads to a downwind fining of the particle size distribution that is commonly observed in dune fields (e.g., Lancaster and Ollier, 1983; Pye, 1985; Sweet et al., 1988).

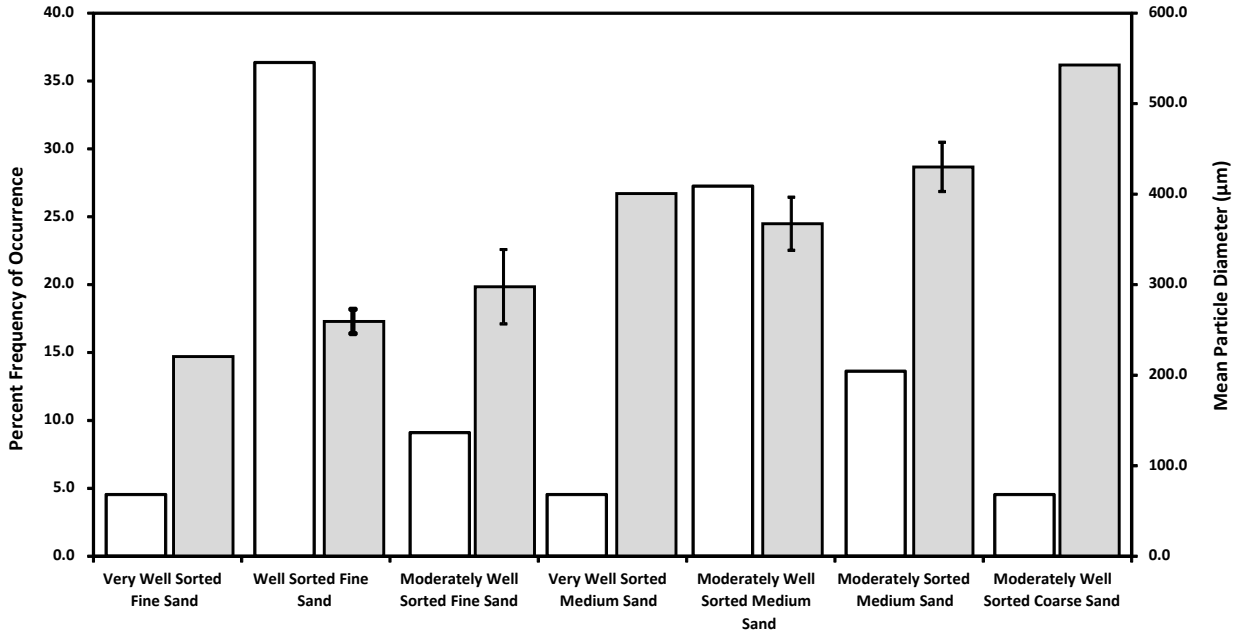

Figure 2. The percent frequency occurrence of sediment type (white bars) and the associated mean grain size (grey bars) for the collected samples in each category. The error bars represent the standard deviation of the mean grain size.

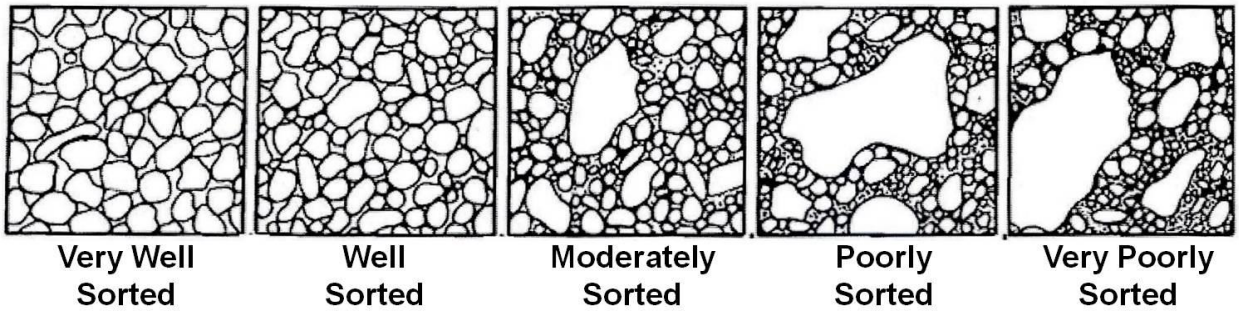

Figure 3. A visual depiction of the grain size distribution characteristic of sorting.

As Fig. 4 shows, for both transects, mean particle diameter increases as a function of increasing distance towards the south of the ODSVRA, terminating in the southern dune preserve area. For both transects the rate of change of the increase in mean particle diameter is similar, with only a 13% difference between mean particle diameters for the samples at ≈500 m and ≈1100 m distances from the shoreline, 8000 m to the south of the northern reference location (the northern part of the northern dune preserve). As reported in Gillies et al. (2014), the wind speed (3 m and 10 m above ground level [a.g.l.]) threshold as determined by the Sensit measurements in the 2013 monitoring study was observed to increase with increasing distance towards the south. The observed change in mean particle diameter

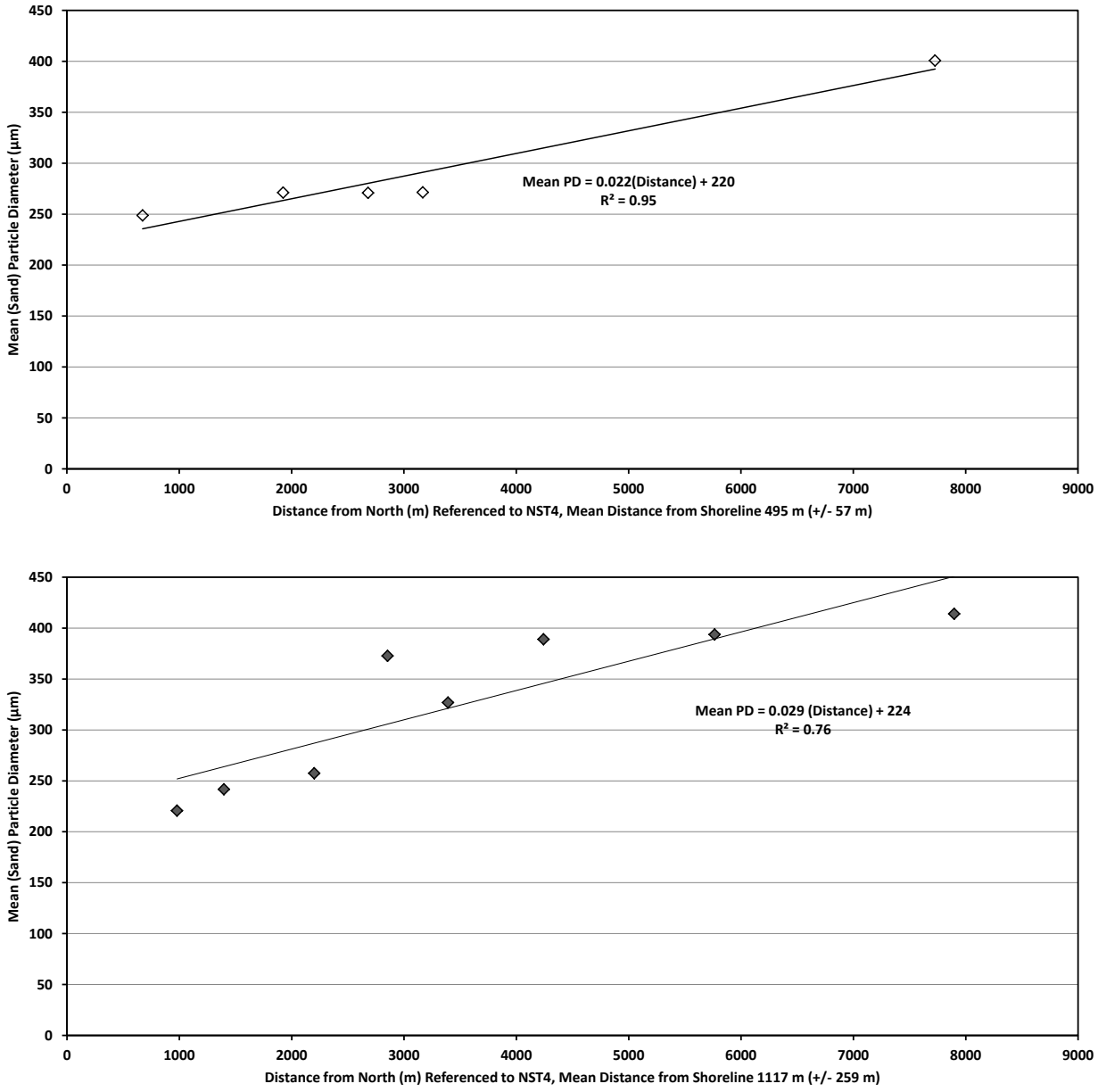

Figure 4. Trends in the mean particle diameter for the sand-sized fraction along two north-south transects. Distance from north is referenced to the sample that is furthest north in the northern dune preserve. The top panel show the trend along a transect approximately 500 m east of the shoreline and the bottom panel shows the trend along a transect approximately 1100 m from the shoreline.

towards the south accounts for the increase in threshold wind speed. The Sensit measurements and analysis indicated threshold 10 m a.g.l. wind speed at the most northerly transect was ≈4.8 m s^{-1} (±0.9 m s^{-1}) and ≈5.6 m s^{-1} (±0.6 m s^{-1}) at the most southerly transect. Applying the Bagnold (1941) threshold expression for the mean particle diameters from north and south:

$$u_{*t} = A\left[\left(\frac{\sigma-\rho}{\rho}\right) gd\right]^{0.5} \quad (1)$$

where: A is a constant (0.1 for air), σ is particle density, ρ is air density, g is the acceleration due to gravity, and d is particle diameter, gives estimates for threshold shear velocities for a 414 µm diameter particle of 0.33 m s^{-1} and 0.24 m s^{-1} for a 230 µm particle. Assuming the aerodynamic roughness length for the S1 Tower can be applied across the dunes these shear velocities can be converted to wind speeds at 10 m a.g.l., which are 8.6 m s^{-1} and 6.4 m s^{-1}, for the larger and smaller diameter particles, respectively. Factoring in the mean percent variation in the particle diameter measurements (37%), the range of 10 m a.g.l. threshold wind speed, based on the Bagnold threshold Eq. (Eq. 1), would be 6.8 m s^{-1} to 10.1 m s^{-1} for the south and 5.1 m s^{-1} to 7.5 m s^{-1} for the north. These ranges are consistent with the threshold wind speed estimates from the Sensit measurements (Gillies et al., 2014). In any case it needs to be noted that the sand is not one size but a distribution and the wind speed that is reported also reflects the average of a distribution over the reporting period (1 hour mean wind speeds were used to define the threshold and cessation of transport). So the measurement-derived values of threshold are lower than those calculated from first principles because they reflect the presence of particles which are smaller than the mean size and hence mobilize at lower wind speeds as well as wind speeds that are higher than the mean value reported.

The trend in mean particle diameter as a function of distance from the shoreline (Fig. 5) is not as well defined as the north-south trends shown in Fig. 4, but a decrease in mean particle diameter with increasing distance from the shoreline is suggested as a general trend. The threshold wind speed data presented in Gillies et al. (2014, their Table 3), also show that in general threshold wind speeds for the easternmost position on the four transects were lower than those in the west, which would reflect the general pattern of particle mean diameter decreasing with increasing distance eastward.

Particles <63 µm in Diameter

The particles <63 µm in diameter represent a very small proportion of the total mass (0.9% to 2.6%) in the dune material (Fig. 6). The samples were typically multi-modal in nature, which does not allow for estimation of descriptors of the distribution based on measurements of central tendency (i.e., mean, standard deviation, skewness, and kurtosis), since those parameters are only really meaningful for unimodal (e.g., normal or log-normal) distributions of particle sizes. To simplify the particle size distribution and get a general idea of the particle size characteristics of this fraction the data were grouped into the following texture categories: Very Fine Sand (VFS, 63 -125 µm), Coarse Silt (CSLT, 31-63 µm), Medium Silt (MSLT, 15.6-31 µm), Fine Silt (FSLT, 7.8-15.6 µm), Very Fine Silt (VFSLT, 3-7.8 µm), Silt-Clay Transition (SCT, 2 -3 µm), and Clay (C, <2 µm) (Folk, 1980). The mean percent frequency of occurrence for each textural class for all samples combined is shown in Fig. 7. The most frequently occurring textural class is clay (30% of sample), followed by very fine silt (20% of sample), and coarse silt (15% of sample).

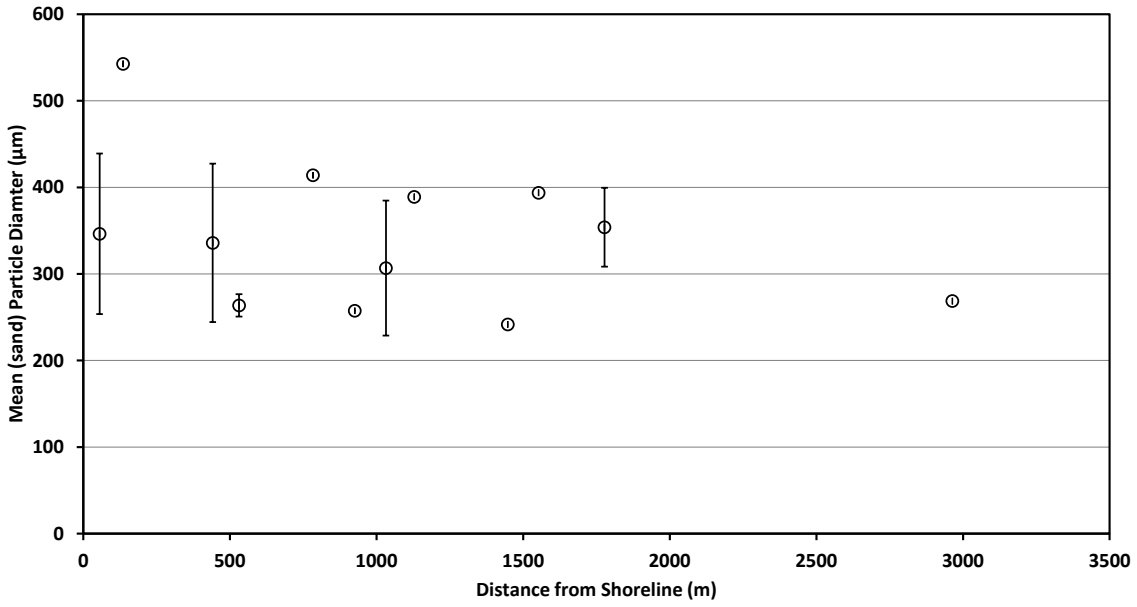

Figure 5. Change in the mean particle diameter for the sand-sized fraction with increasing distance from the shoreline, suggesting a decrease with increasing distance to the east.

The fine tail of particles (<63 µm) is dominated by the clay fraction that, averaged for all samples, composes ≈30%. Recall however, that the particles <63 µm are, on average, 1% of the total mass of an average sample. Because it is defined with an aerodynamic diameter limit of 10 µm, the PM_{10}, assuming that it existed as unconsolidated or individual particles would reside in the size range <6.15 µm physical diameter. The aerodynamic diameter is a function of the physical size of the particle and its density (and shape, but that is not factored in here):

$$PM_{10} \approx Particle\ Diameters\ (< 6.15\ \mu m) \times \sqrt{\frac{Particle\ Density\ (2650\ kg\ m^{-3})}{Water\ Density\ (1000\ kg\ m^{-3})}} \qquad (2)$$

Here the particle density is assumed to be that of quartz.

The particle size data can be aggregated in multiple ways. Two obvious aggregations are along the east-west and north-south directions. The mean percent of the sample for each of the textural designations as a function of (approximate) distance from the shoreline excluding the dune preserves (north and south) is shown in Fig. 8.

Some trends can be observed in these data, but none are statistically significant. It appears that there is an increase in the C content from the shoreline to approximately 1335 m (±38 m). The VFS and CSLT percent increases between 1335 m (±38 m) and 2500 m (±405 m), suggesting a slight coarsening in the fine material towards the east past 1335 m.

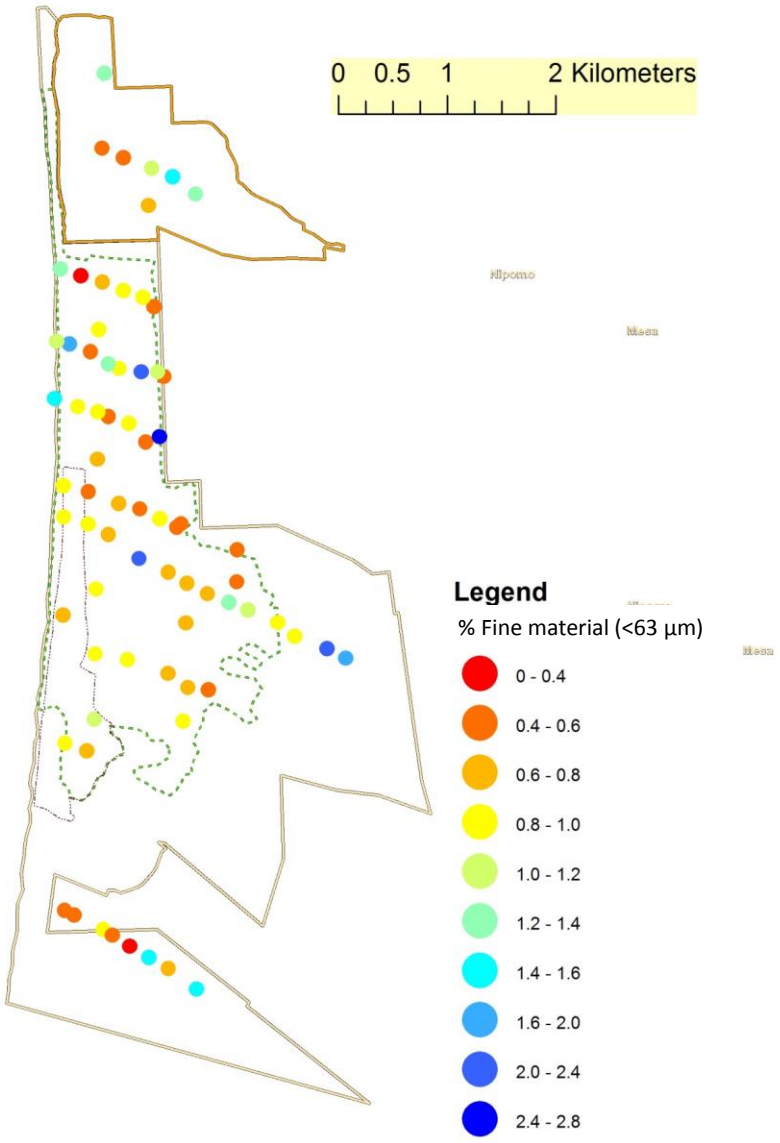

Figure 6. The percent of sediment <63 µm in the samples collected for particle size analysis.

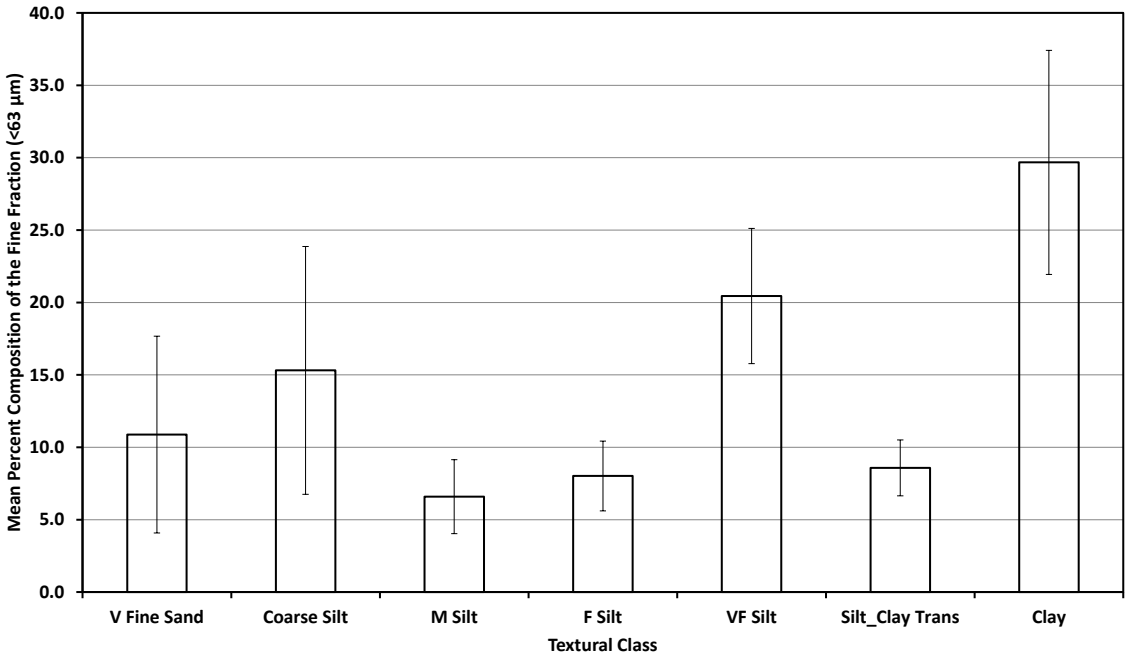

Figure 7. The mean percent sample composition as a function of textural class based on 91 samples. The error bar represents the standard deviation of the mean.

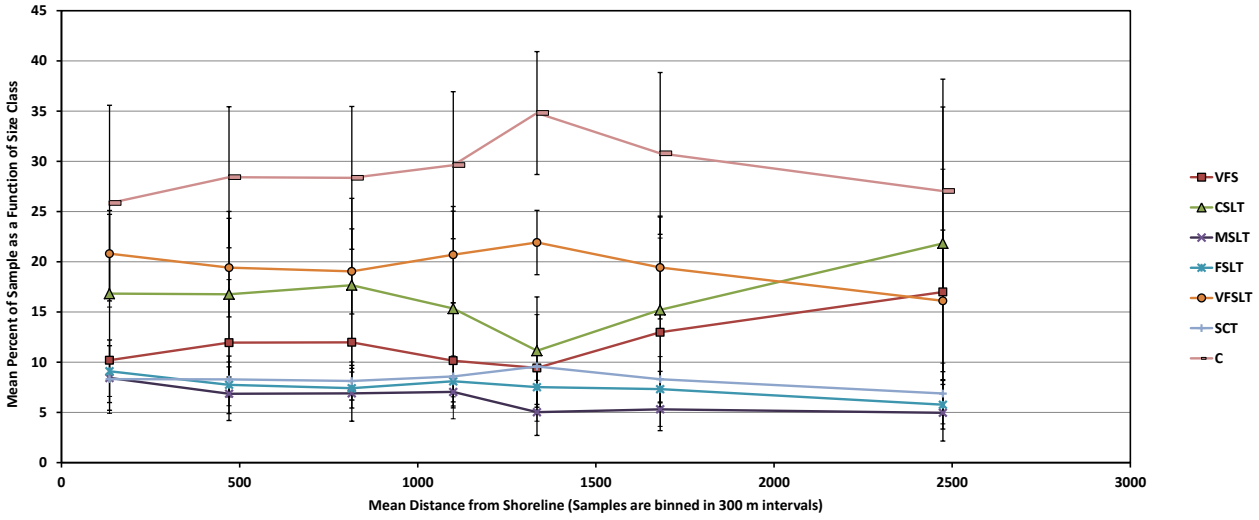

Figure 8. The mean percent of the sample for each of the textural designations as a function of (approximate) distance from the shoreline for samples in the ODSVRA. The texture symbols (size class) are: very fine sand (VFS), coarse silt (CSLT), medium silt (MSLT), fine silt (FSLT), very fine silt (VFSLT), silt-clay transition (SCT), and clay (C). Data shown do not include samples from Dune Preserve in North or Oso Flacco in South.

The change in texture as a function of distance from the shoreline for the north and south dune preserve areas is shown in Fig. 9. In both preserve areas and the park proper, the smallest percent fluctuation as a function of texture and distance from the shoreline is observed for the MSLT, FSLT, and SCT. In both cases (and for the ODSVRA samples) the largest fluctuations in texture are observed for the VFS, CSLT, VFSLT, and C components. In the Oso Flaco preserve the very fine sand (VFS) and coarse silt (CSLT) percentages both increase generally towards the east, suggesting that the material is becoming increasingly coarser in this small fraction of the total material, which could indicate a winnowing of the finer fractions. The north preserve data do not show any consistent spatial trends.

The percent of the sample (individual samples, i.e., no grouping of data points) represented by the different size classes for two north-south transects at different distances from the shoreline are shown in Fig. 10. Both transects show, in general an increase in the C content with increasing distance to the south to a distance of approximately 3000 m from the northern points of reference. This approximates the position of the S1 tower. There is a noticeable dip in the clay content at ≈4000 m (Fig. 10A) and 2000 m (Fig. 10B), but it increases again by the next sample locations.

The MSLT, FSLT, and SCT along the ≈500 m from the shoreline transect generally decrease to 2700 m then show a steady increase with increasing distance to the south. This trend is not obvious for the transect further inland, ≈1000 m from the shoreline.

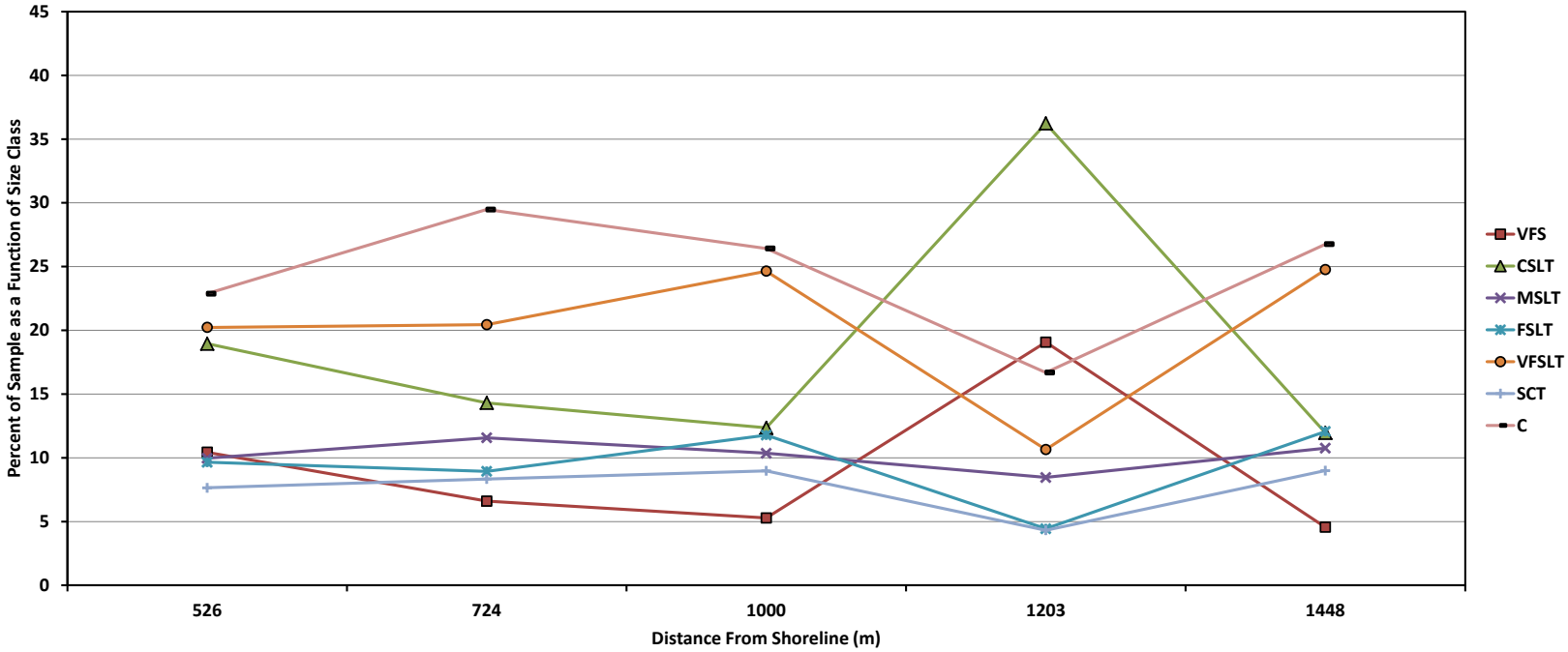

Figure 9A. The percent of the sample for each of the textural designations as a function of (approximate) distance from the shoreline for the north preserve. The texture symbols (size class) are: very fine sand (VFS), coarse silt (CSLT), medium silt (MSLT), fine silt (FSLT), very fine silt (VFSLT), silt-clay transition (SCT), and clay.

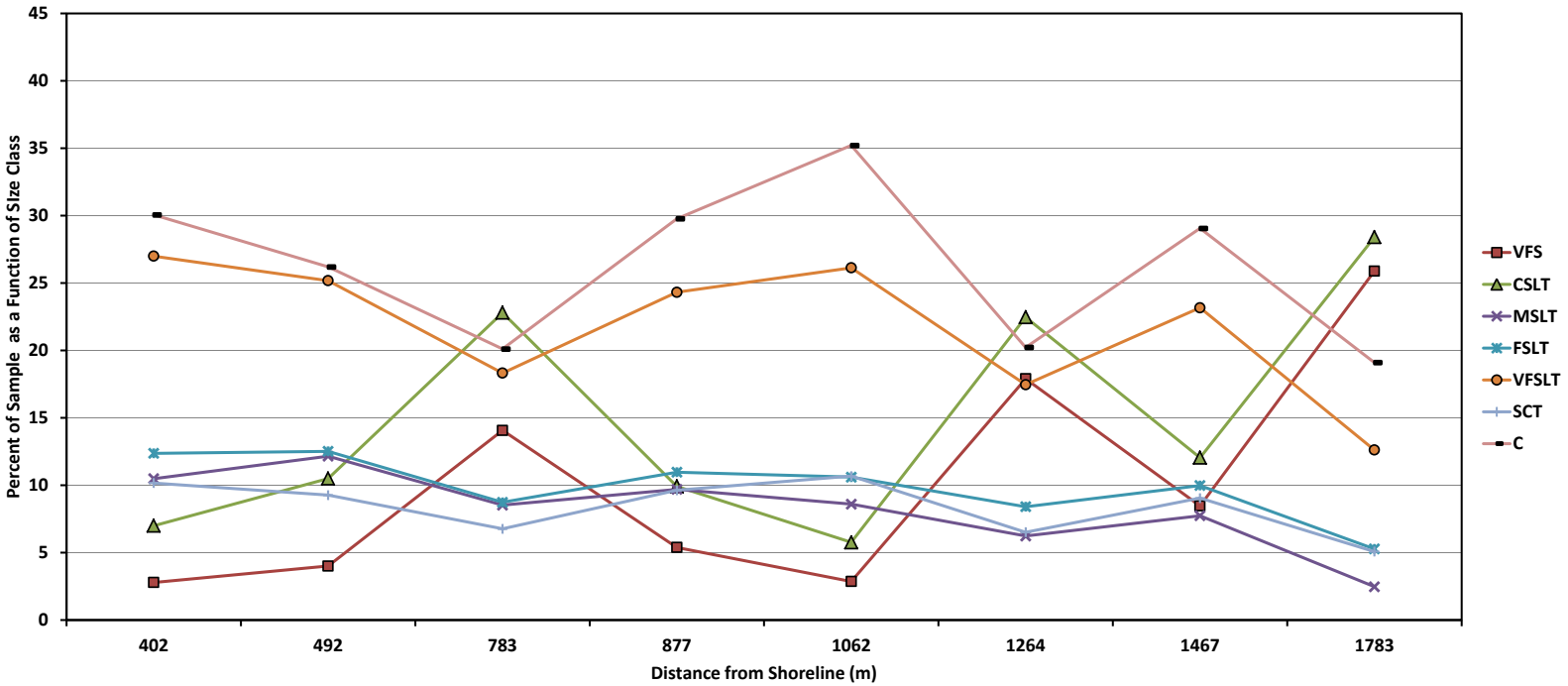

Figure 9B. The percent of the sample for each of the textural designations as a function of (approximate) distance from the shoreline for the Oso Flaco preserve (bottom panel). The texture symbols (size class) are: very fine sand (VFS), coarse silt (CSLT), medium silt (MSLT), fine silt (FSLT), very fine silt (VFSLT), silt-clay transition (SCT), and clay.

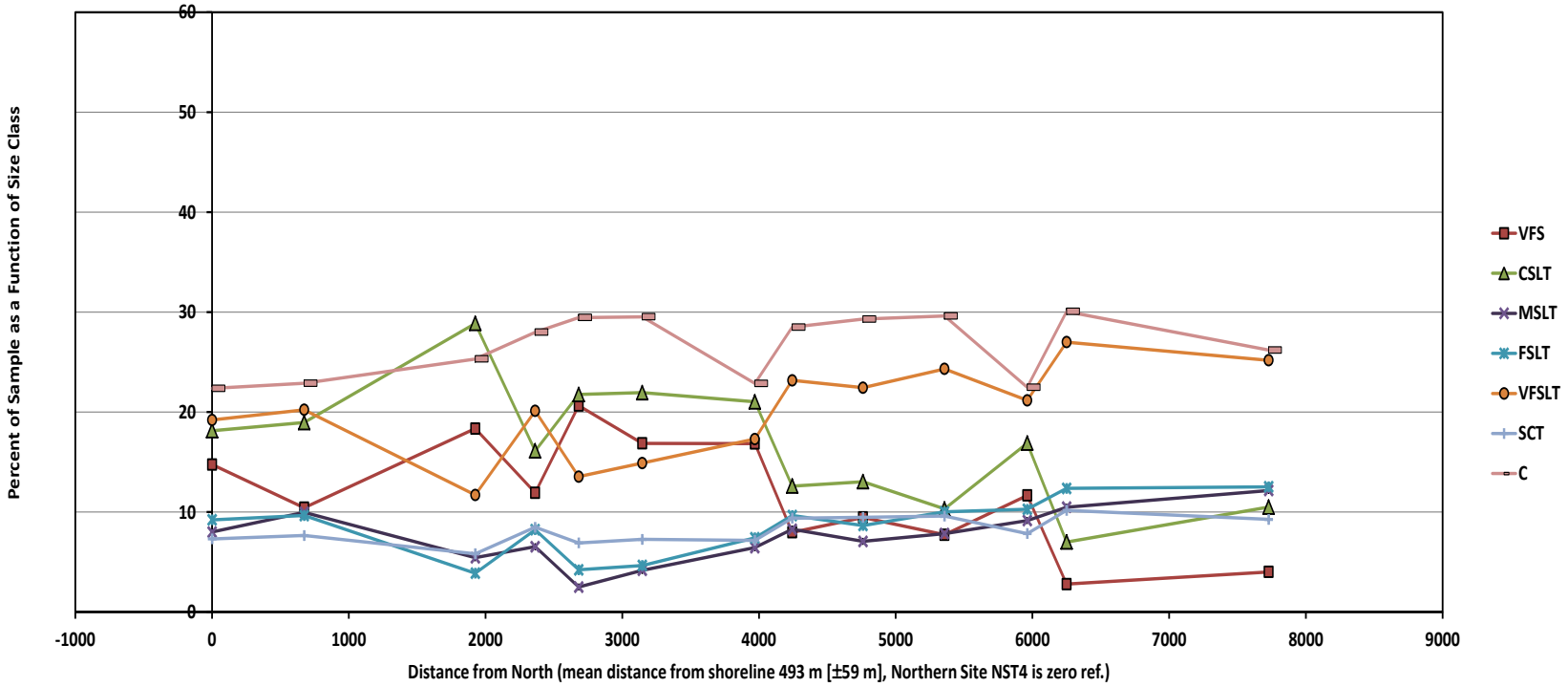

Figure 10A. The percent of the sample for each of the textural designations along a north-south transect for (single samples) between ≈402 m and ≈596 m (mean distance=498 m) beginning at the northernmost sand sample collection location in the northern dune preserve (Lat: 35.07875 N, Long: 120.6293 W).

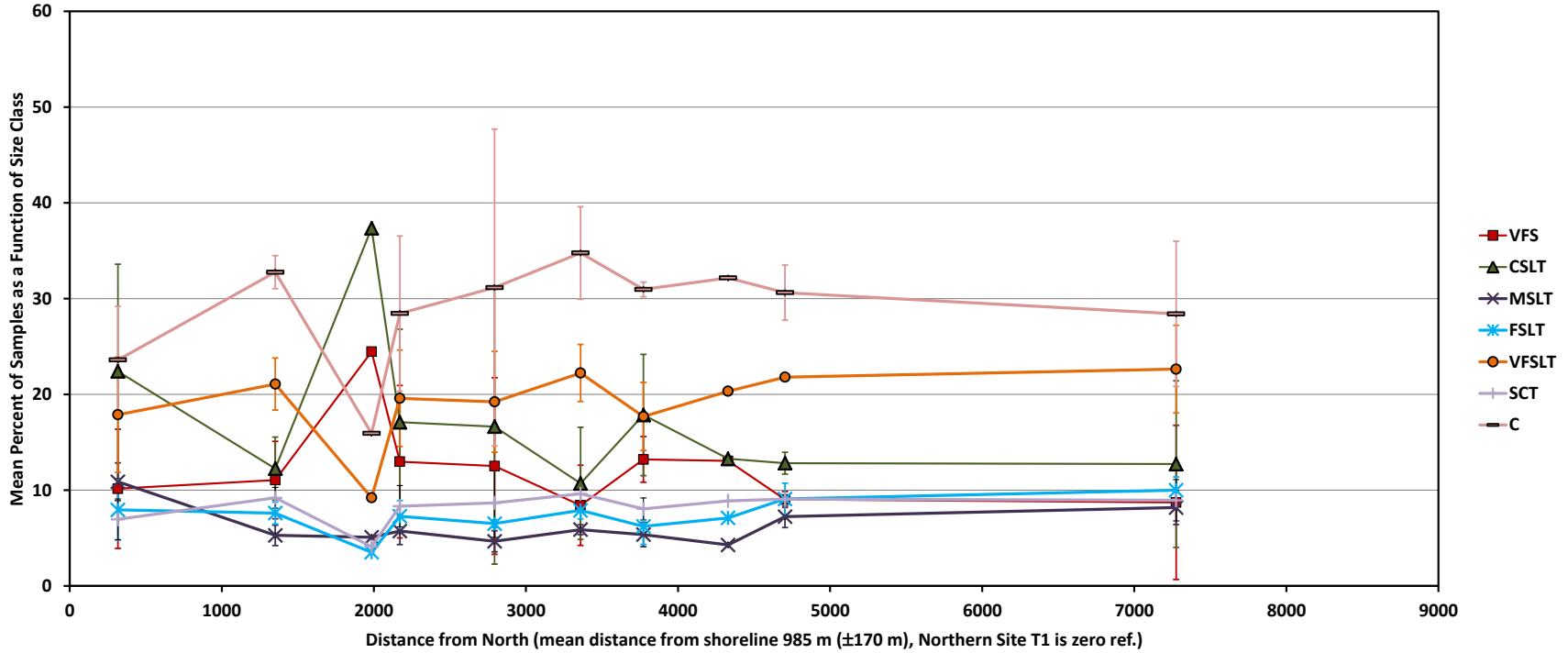

Figure 10B. The percent of the sample for each of the textural designations along a north-south transect for (single samples) between ≈722 m to ≈1278 m from the shoreline (mean distance=985 m). The texture data in this Figure represent averages made by combining data in approximately 500 m wide bins to smooth out the pattern (error bars show the standard deviation of the mean). For this transect position north-south is referenced to the northern position of Transect T1. The texture symbols (size class) are: very fine sand (VFS), coarse silt (CSLT), medium silt (MSLT), fine silt (FSLT), very fine silt (VFSLT), silt-clay transition (SCT), and clay.

Particle Size and PI-SWERL™ Emissions

The PI-SWERL™ data provide a means to compare emissions produced for surfaces that have different proportions of the fine (<63 μm) and coarse fractions (>63 μm) of the dune sediments. To evaluate if there are relationships between the particle size data and the emission of PM_{10} as measured with the PI-SWERL™ the particle size data were aggregated in various ways to determine if the relative amounts of the fine and coarse materials could explain, in part, the strength of the dust emissions as a function of wind shear. As described earlier the PM_{10} in the fine material could exist as individual particles that are released once saltation begins, or they are formed as larger particles break down during the vigorous saltation process, or a combination of both.

If PM_{10} particles were mixed into the dunes as individual, free particles then PM_{10} released as dust during wind events would potentially include all particles <6.15 μm. To get a percentage of the PM_{10} in each of the samples collected for PSD analysis, the fractions for all particles less than this diameter were summed to estimate the percent of PM_{10}. Two additional aggregations of the PSD data were calculated as well, the sum of the %SCT and %C particles (<2.75 μm), and the sum of the %C. The rationale being that these are the most likely components of the fine size fraction (<63 μm) that could correlate to the strength of dust emissions. Each of these groups of PSD data are compared to the PI-SWERL emissions measured at the site where the samples were collected in Figs. 11, 12, and 13. As these Figs. indicate there is a high degree of variability in these comparisons and there is no indication of a link between these specific characteristics of the fine fraction PSD (i.e., contained within the <63 μm diameter particles) for the collected samples and the strength of the dust emissions as measured with the PI-SWERL.

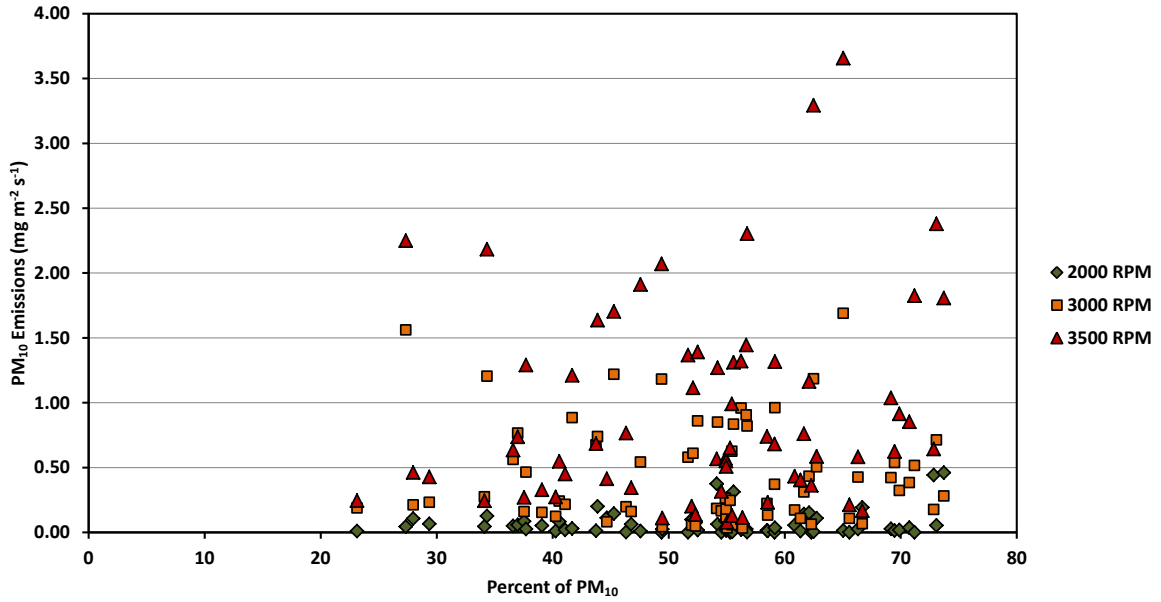

Figure 11. PM_{10} Emissions plotted against the percent of PM_{10} sized particles (<6.15 µm) in the fine fraction of the sediment samples.

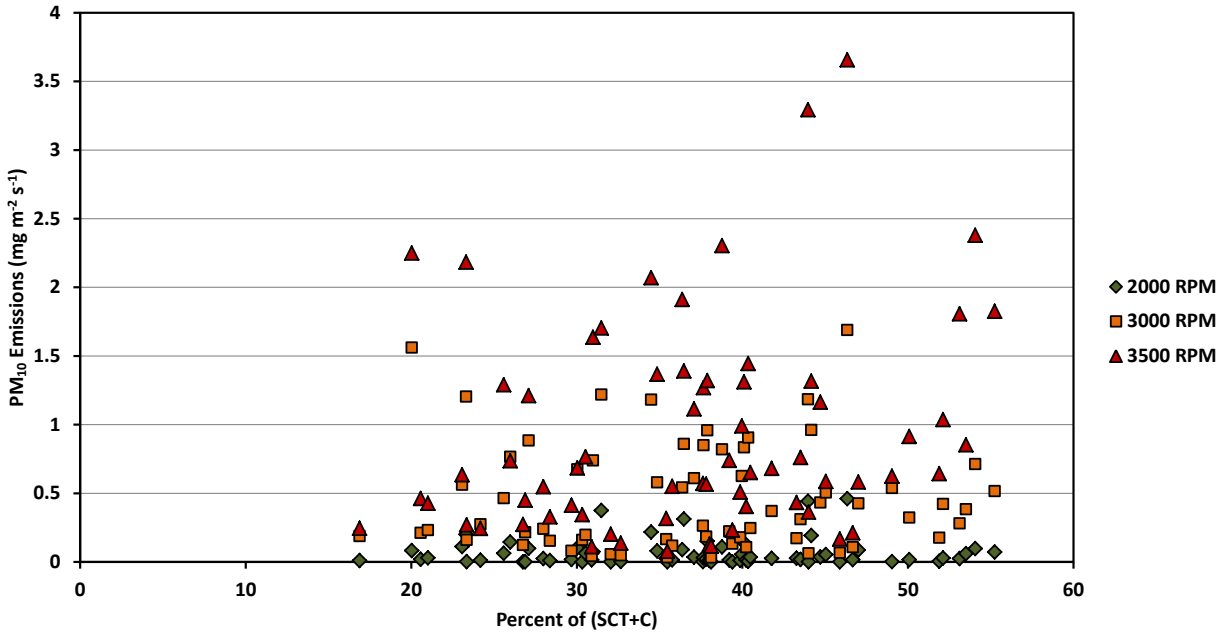

Figure 12. PM_{10} Emissions plotted against the sum of %SCT and %C in the fine fraction of the sediment samples.

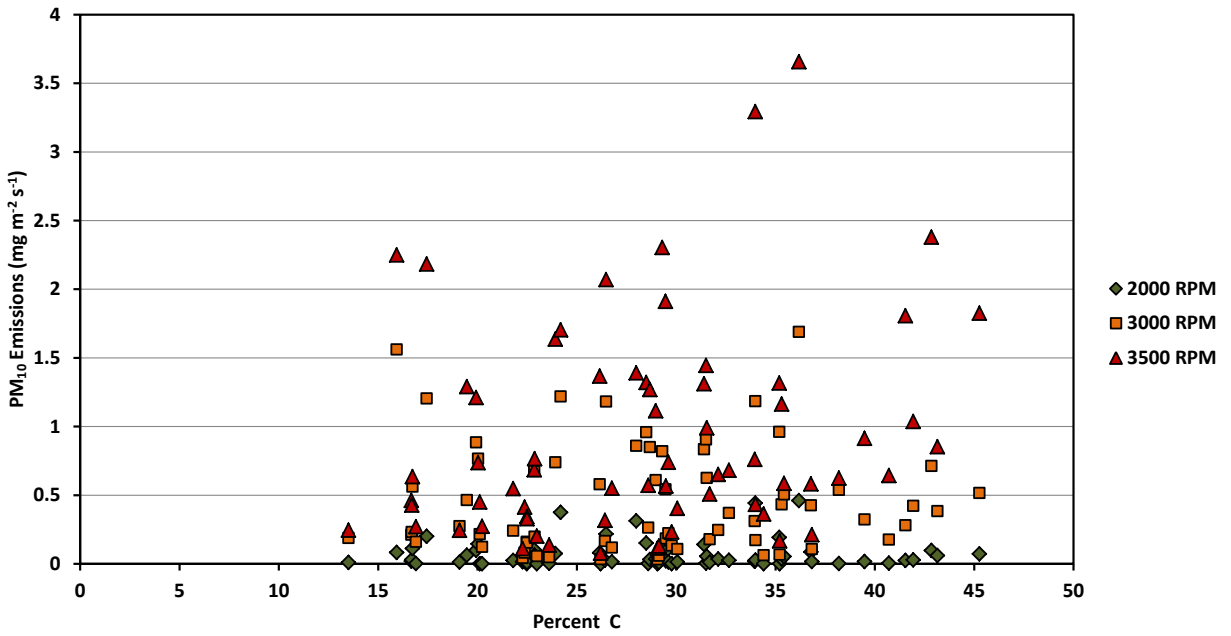

Figure 13. PM_{10} Emissions plotted against the percent of %C in the fine fraction of the sediment samples.

The relative amounts of the fine particle fraction (i.e., contained within the <63 µm diameter particles) are not the only influence on the strength of the dust emissions, the sand fraction (>63 µm) plays a role as well. In general, the smaller the sand sized particles the lower is the threshold shear velocity needed to mobilize the sand; there is a relationship between the sand sized particles and their ability to modulate the dust emissions (Gillette and Chen, 1999). The effect of sand size on threshold shear velocity and PM_{10} emissions is shown in Fig. 14. As the fraction of coarse sand increases in the sediment, Fig. 14 shows that the threshold shear velocity increases (as determined from PI-SWERL™ measurements). This also corroborates the threshold wind speed estimates from the transect measurements, where coarsening of the particle size towards the south results in an increase in threshold wind speed. For each of the shear velocity conditions during a PI-SWERL™ test, Fig. 14 also demonstrates that the coarsening of the sand in the samples collected (i.e., the size distribution shifts to larger particle diameters), is associated with a decrease in the PM_{10} emissions. These two observations may be reconciled by noting that all else being equal, for a given wind speed (or shear velocity) a higher threshold shear velocity results in lower PM_{10} emissions.

As shown in Fig. 15 as the fraction of fine sand increases in proportion to the medium sand the threshold shear velocity decreases and the emissions of PM_{10} increases for each of the three shear velocity conditions during a PI-SWERL™ test.

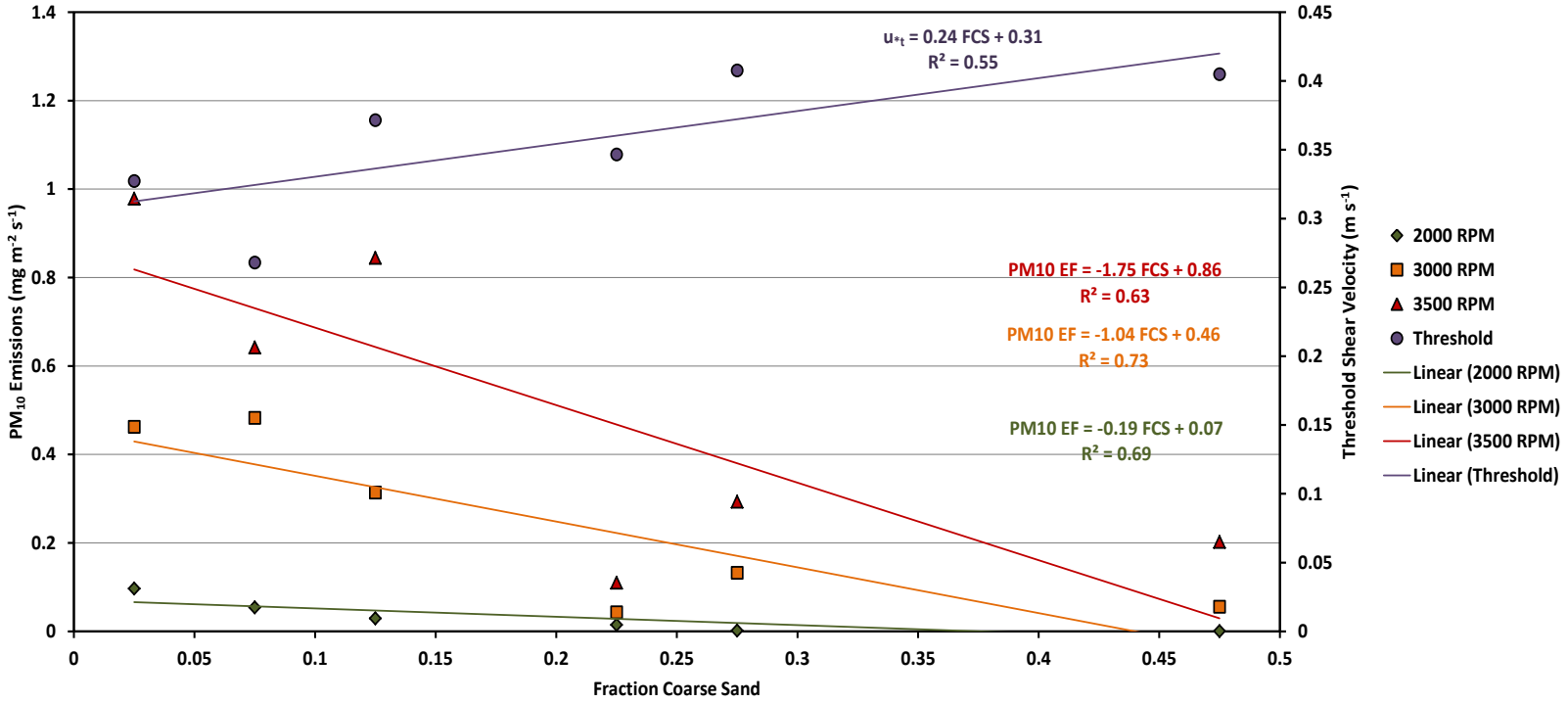

Figure 14. Relationships between PM_{10} emissions and the fraction of coarse sand in the sediment samples.

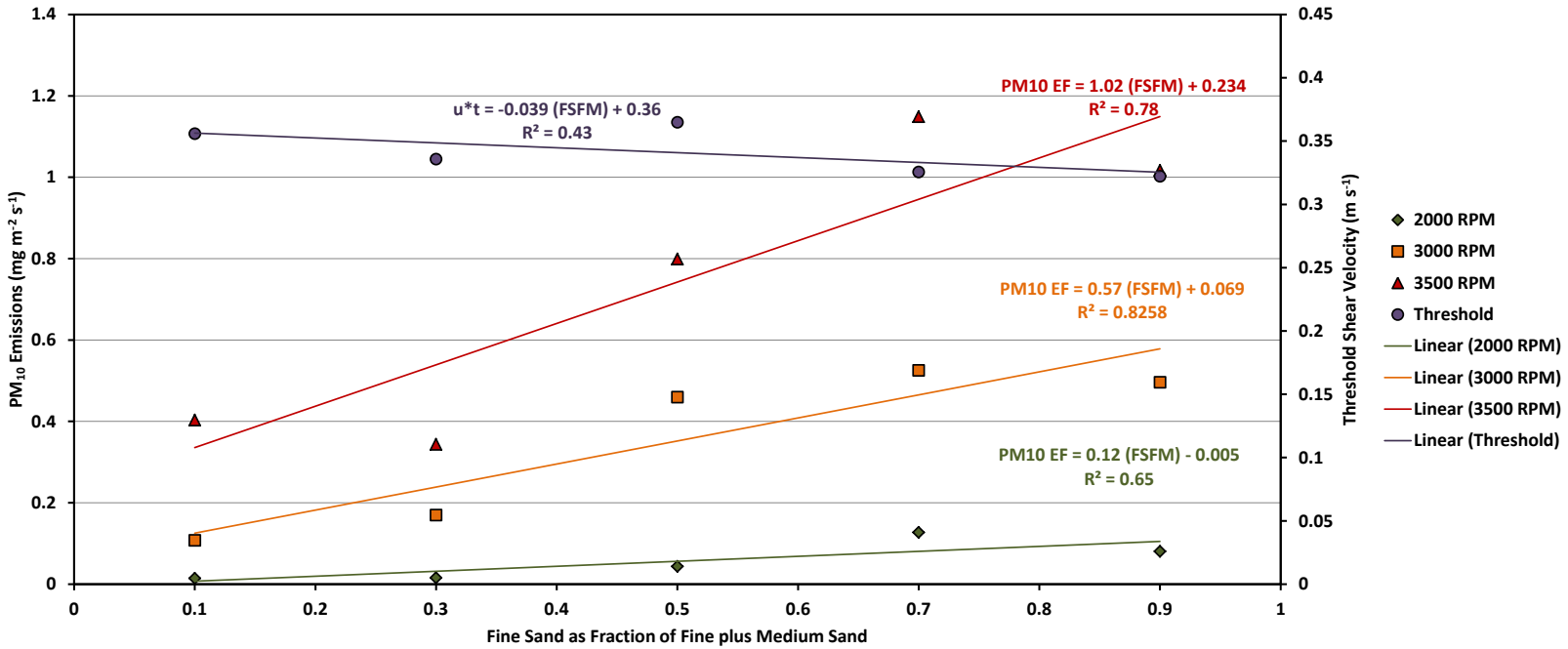

Figure 15. Relationships between PM_{10} emissions and the ratio of FS/(FS+MS).

Discussion

Based on the information portrayed in Figs. 11, 12, 13, 14 and 15, maps were created that show the spatial distribution of the identified particle size characteristics. Figure 16 shows the spatial distribution of the percentage of PM_{10} (i.e., particles <6.15 μm diameter), Fig. 17 the percentage of C in the fine sediments, Fig. 18 the percentage of coarse sand particles, and Fig. 19 the ratio of FS/(FS+MS). There is considerable variation in these properties of the sediments across the space of the ODSVRA and dune preserves, which is indicative of the dynamic nature of this coastal dune environment. These figures, however, suggest that increased PM_{10} emissions as measured with the PI-SWERL™ are associated with areas with lower threshold shear velocities for sand movement, which implies smaller mean particle diameter for this size fraction (i.e., >63 μm).

The particle size data for the sand sized fraction are consistent with the PI-SWERL™ results (Etyemezian et al., 2014) and the results of the temporary monitoring program carried out in 2013 (Gillies et al., 2014) in that they provide an explanation as to why the threshold shear velocities increase towards the south. This increase in threshold shear velocity (for sand particles) is due principally to the observed increase in mean particle diameter of the sand-sized fraction (Fig. 4). The relationship between the sand-sized fraction of the PSD (i.e., Figs. 14 and 15) and threshold shear velocity also indicates that as threshold wind shear decreases, there is an increase in the associated PM_{10} emissions. The relationship between the particle size characteristics of the fine fraction (<63 μm) of the samples and the strength of the PI-SWERL™ measured emissions is not as clear (see Figs. 11-13) as with larger sand grains.

It needs to be noted that considerable variation in the spatial patterns of the grain size distribution can be expected across several physical scales. In the west to east direction, grain size characteristics will change based on their position across the dunes. For example, in the lee of dunes there may be enrichment of fine particles in the zone of reduced wind speed past dune crests. These finer scale patterns are not well-captured by the distribution of samples selected for analysis, nor are the PI-SWERL™ measurements at a sufficiently distance-resolved grid to capture variation in emissions at length scales that may be <100 m.

We believe that considering all data, i.e., temporary monitoring, PI-SWERL™, and particle size data, that a picture has emerged that generally describes the spatial variability of the PM_{10} emissions. The PM10 emissions measured with the PI-SWERL show a pattern that is corroborated by the temporary monitoring networks, with higher PM10 measurements on Transects T2 and T3, being associated with areas that the PI-SWERL measurements have identified as having higher emission potential. The PSD data, although showing a high degree of variability across space, do indicate that the areas of higher emission potential are associated with areas that have lower threshold shear velocity (based on the >63 μm fraction), which also correspond to areas with higher PI-SWERL measured emission potential.

What remains unresolved is the causal mechanism that explains these observations. The particle size and PI-SWERL data, when taken together (Figs. 11-13), suggest that hypothesis one, which stated that the strength of the PM_{10} emissions would increase (for equivalent shear stresses) as the fraction of the total mass of silt and clay increased with respect to the sand sized component (>63 μm) is not explanatory. If hypothesis one was correct, a link between the amount of the fine particle material <6.12 μm (i.e., the PM_{10} fraction) and the strength of the PM_{10} emissions (for equivalent shear stresses)

should have been revealed in the data. This did not occur as shown in Figs. 11-13. The physics of the PM_{10} release from the sediment of the ODSVRA appears to be more complicated than this simple model. However, the correlations demonstrated between characteristics of the sand sized component of the ODSVRA sediments and PM_{10} emissions (Figs. 14 and 15) suggest that the physics of the emission process is controlled primarily by the movement (threshold, transport, and saltation dynamics) of this size fraction of the PSD, rather than the PSD and mass fraction associated with the fine fraction (<63 µm). How the emission of PM_{10} from the sediment, once saltation is initiated, is influenced by the particle size distribution of the sand-sized component and the fine sediment fraction (<63 µm) is not known at this time.

It seems more likely that hypothesis three, that it is a combination of the reservoir and the breakdown of particles during saltation, which appears to be enhanced as the overall particle size distribution of the >63 µm fraction shifts to a smaller mean diameter offers a more plausible explanation. There is however, insufficient information to accept or reject this hypothesis. It is not well-understood which particle size or size range is more or less susceptible to dust-sized particle production during saltation and abrasion. Bullard et al. (2004), however, noted that production of fine particles (including 10 µm particles) was less for sands that had particle diameters <250 µm removed by sieving than samples that did not. The creation of dust –sized particles by abrasion of sand-sized particles should be enhanced as sand particles become more angular. Orme and Tchakerian (1986) noted that sand grains in the Santa Maria/Guadalupe dunes were mostly sub-angular to angular, suggesting that the sand within the ODSVRA are also likely dominated by angular forms. Finally, the underlying physics of the dust emission system within the ODSVRA remains unresolved. The source of the PM_{10} may be due to micro-scale processes of dust generation, larger scale processes created by the dunes being out of equilibrium, or a combination of both, but the underlying cause of why the Oceano dunes produce dust at the levels observed remains to be determined.

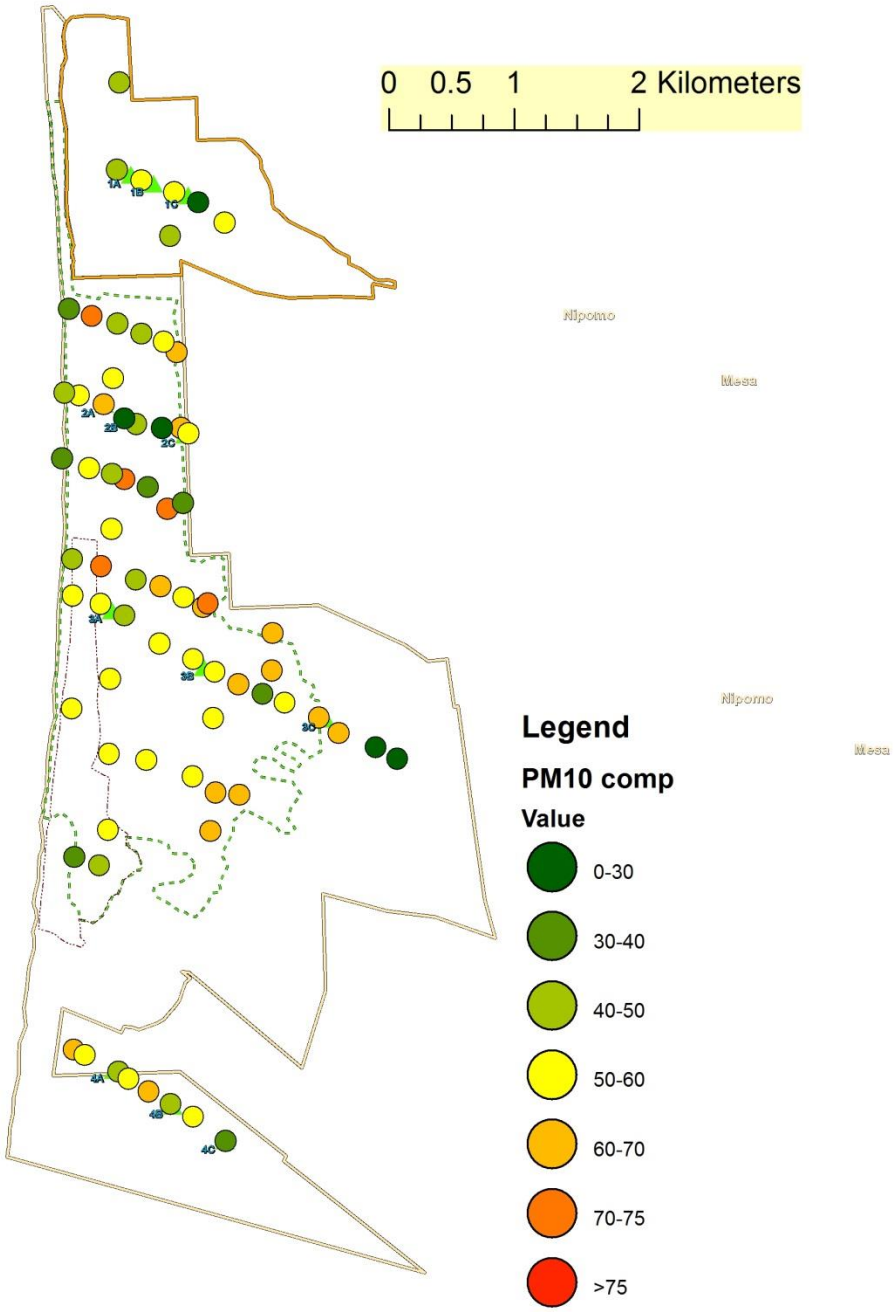

Figure 16. The percent of the fine fraction (<63 µm) that is PM_{10} (i.e., <6.15 µm).

Figure 17. The percent of the fine fraction (<63 µm) that is clay size (<2 µm).

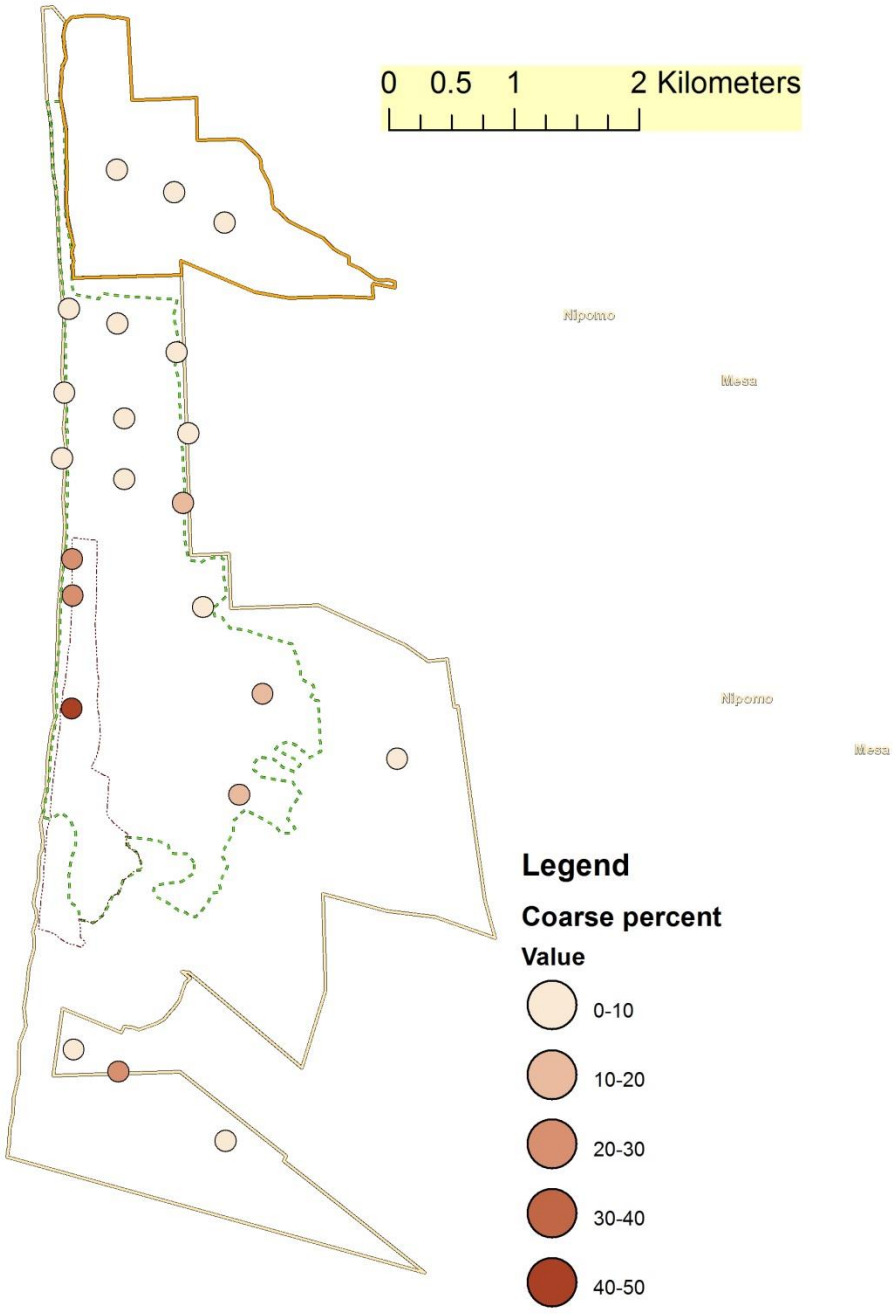

Figure 18. The percent of the sand fraction (>63 µm) that is coarse sand (500 - 1000 µm).

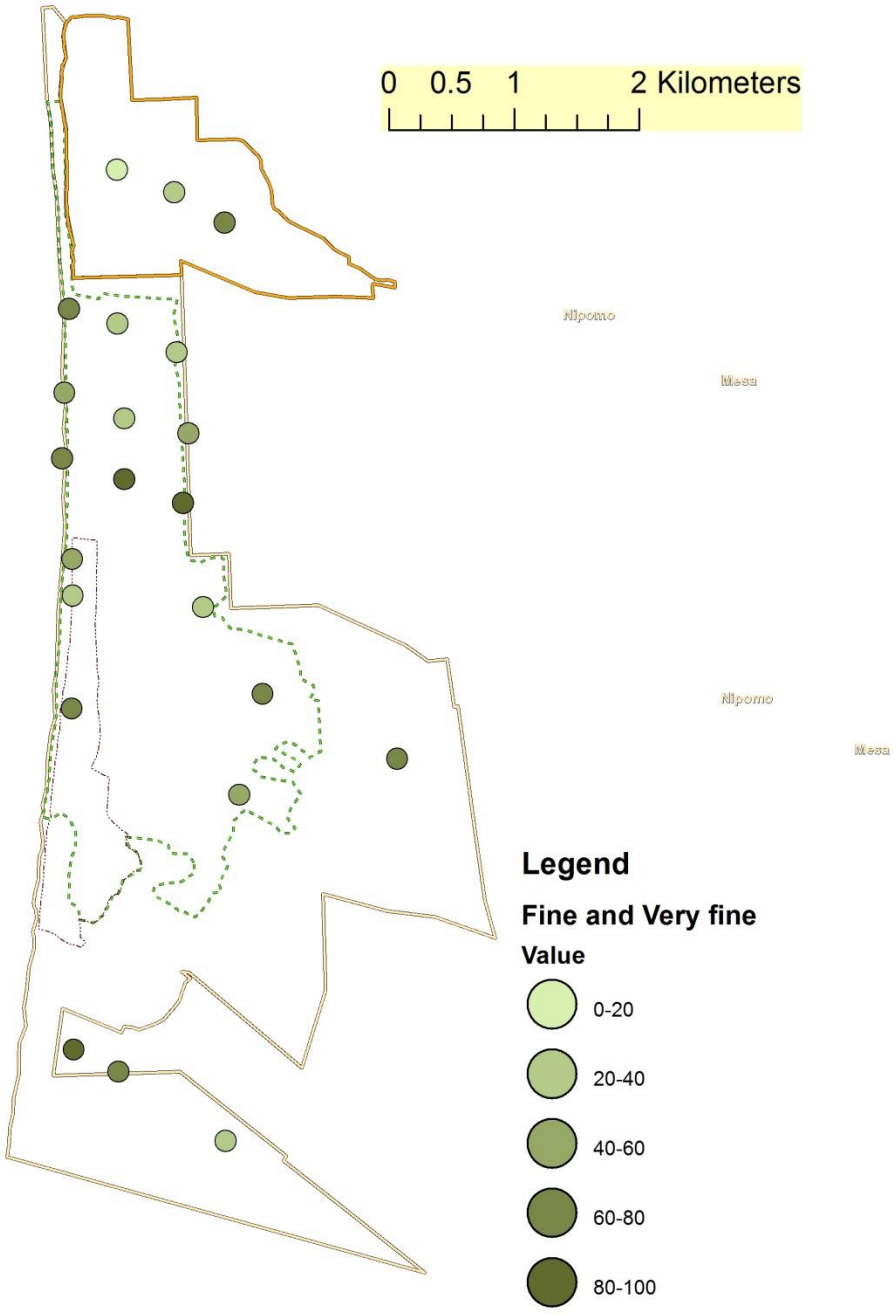

Figure 19. The ratio (expressed as %) of FS/(FS+MS) in the sand-sized fraction (>63 µm) of the samples.

References

Alfaro, S.C., J.L. Rajot, and W.G. Nickling (2004), Estimation of PM20 emissions by wind erosion: main sources of uncertainties, *Geomorphology*, *59*(1-4), 63-74.

Bagnold, R.A. (1941), *The Physics of Blown Sand and Desert Dunes*, 265 pp., Chapman and Hall, London.

Blott, S.J., and K. Pye (2001), GRADISTAT: A grain size distribution and statistics package for the analysis of unconsolidated sediments, *Earth Surface Processes and Landforms*, *26*(11), 1237-1248.

Bullard, J.E., and K. White (2005), Dust production and the release of iron oxides resulting from the aeolian abrasion of natural dune sands, *Earth Surface Processes and Landforms*, *30*(1), 95-106.

Bullard, J.E., G.H. McTainsh, and C. Pudmenzky (2004), Aeolian abrasion and modes of fine particle production from natural red dune sands: an experimental study, *Sedimentology*, *51*(5), 1103-1125.

Bullard, J.E., G.H. McTainsh, and C. Pudmenzky (2007), Factors affecting the rate and nature of fine particle production by aeolian abrasion, *Sedimentology*, *54*, 1169-1182.

Eshel, G., G.L. Levy, U. Mingelgrin, and M.J. Singer (2004), Critical evaluation of the use of laser diffraction for particle-size distribution analysis, *Soil Science Society of America Journal*, *68*, 736-743.

Etyemezian, V., J.A. Gillies, D. Zhu, A. Pokharel, and G. Nikolich (2014), 2013 Intensive Wind Erodibility at and Near the Oceano Dunes State Vehicular Recreation Area: Preliminary Report of Findings, Report prepared for California Department of Parks and Recreation, Pismo Beach, CA.

Etyemezian, V., J.A. Gillies, M. Shinoda, G. Nikolich, J. King, and A.R. Bardis (2014), Accounting for surface roughness on measurements conducted with PI-SWERL: Evaluation of a subjective visual approach and a photogrammetric technique, *Aeolian Research*, *13*, 2014.

Etyemezian, V., G. Nikolich, S. Ahonen, M. Pitchford, M. Sweeney, J. Gillies, and H. Kuhns (2007), The Portable In-Situ Wind Erosion Laboratory (PI-SWERL): a new method to measure PM_{10} windblown dust properties and potential for emissions, *Atmospheric Environment*, *41*, 3789-3796.

Gillette, D.A. (1976), Production of fine dust by wind erosion of soil: Effect of wind and soil texture, Report prepared for U.S. Energy Research and Development Administration, Oak Ridge, Tennessee, 591-609.

Gillette, D.A. (1978), A wind tunnel simulation of the erosion of soil: effect of soil texture, sandblasting, wind speed, and soil consolidation on dust production, *Atmospheric Environment*, *12*, 1735-1743.

Gillette, D.A., and W. Chen (1999), Size distributions of saltating grains; an important variable in the production of suspended particles., *Earth Surface Processes and Landforms*, *24*(5), 449-462.

Gillies, J.A. and V. Etyemezian (2014) Wind and PM_{10} Characteristics at the ODSVRA from the 2013 Assessment Monitoring Network. Report prepared for California Department of Parks and Recreation, Pismo Beach, CA.

Kok, J.F. (2011), A scaling theory for the size distribution of emitted dust aerosols suggests climate models underestimate the size of the global dust cycle, *Proceedings of the National Academy of Sciences of the United States of America*, *108*(3), 1016-1021.

Lancaster, N., and C. D. Ollier (1983), Sources of sand for the Namib Sand Sea, *Zeitschrift für Geomorphologie*, *Supplementband 45*, 71-83.

Nickling, W.G., and J.A. Gillies (1989), Emission of fine-grained particulates from desert soils, in *Paleoclimatology and Paleometeorology: Modern and Past Patterns of Global Atmospheric Transport*, M. Leinen and M. Sarnthein (eds.), pp. 133-165, Kluwer Academic Publishers.

Orme, A. R. and V. P. Tchakerian (1986), Quaternary dunes of the Pacific Coast of the Californias, in *Aeolian Geomorphology*, W. G. Nickling (ed.), 149-175, Allen and Unwin.

Pye, K. K. (1985), Controls on fluid threshold velocity, rates of aeolian sand transport and dune grain size parameters along the Queensland coast, paper presented at Proceedings of International Workshop on the Physics of Blown Sand, University of Aarhus, Aarhus.

Rajot, J.L., S.C. Alfaro, L. Gomes, and A. Gaudichet (2003), Soil crusting on sandy soils and its influence on wind erosion, *Catena*, *53*, 1-16.

Sweet, M. L., J. Nielson, K. Havholm, and J. Farralley (1988), Algodones dune field of southeastern California: case history of a migrating modern dune field, *Sedimentology*, *35*(6), 939-952.